

MAGNETIC RESONANCE IMAGING OF CONCRETE WITH FRP REINFORCEMENT

Emanuele MARFISI

Chris BURGOYNE

Department of Engineering, University of Cambridge, UK

Keywords: aramid FRP, magnetic resonance imaging.

1 INTRODUCTION

Engineers have long wanted to see inside concrete non-destructively. Techniques such as CT scanning with X-rays, which relies on density differences in the sample, and Magnetic Resonance Imaging, which can locate water within a sample, are both potential candidates. However, the density variation in concrete is small, so CT scans show very little, and the presence of iron in rebar distorts an MRI image. But aramid FRP reinforcement is non-magnetic. When combined with white limestone aggregate, which also does not distort the image, it is possible to non-destructively image a concrete sample immediately after casting (so the aggregate distribution can be studied), and also when hardened, both before, during and after loading. This allows the progress of cracking to be followed. This paper summarises the results of a study, the objectives of which were to show that it is possible to determine the state of cracking within a concrete sample, and to correlate this with the location of the aggregate within the concrete. Three papers have been published which give full details of the study [1, 2, 3]. The work reported here has been undertaken at Cambridge as a joint project between the Cambridge University Engineering Department (CUED) and the Herchel Smith Laboratory for Medicinal Chemistry (HSLMC).

2 MAGNETIC RESONANCE IMAGING

MRI allows the direct, non-destructive observation of both static and dynamic phenomena of fluid transport in porous media. For this reason its development has led to application in many different fields. It is appropriate here only to give a brief overview of MRI principles; for full details of the technique the reader is directed to the specialist literature (e.g. for medical applications [4]; for non-medical applications [5]). Magnetic resonance involves the simultaneous application of a static magnetic field and pulses of radio-frequency to a sample; the magnetic field aligns all the hydrogen nuclei that are present in the sample and the radio-frequency pulse changes that orientation. As the hydrogen nuclei return to their original equilibrium state, they generate a signal which is detectable by a sensitive radio-frequency receiver and is proportional to the density of hydrogen nuclei and therefore, indirectly, to the local water content. Applying a magnetic field gradient in a defined direction gives the signal spatial discrimination. In this way it is possible to define the local orientation of a two-dimensional (2D) slice and then to measure the spatial distribution within it. Alternatively a complete three-dimensional (3D) assessment can be made. The signal is also affected by the mobility of the hydrogen nuclei; although liquid water gives an MRI signal, its low mobility in ice prevents any signal detection. Consequently, the observation of the different internal structures inside an object depends not only on the amount of water present but also on its mobility.

Water in porous media is generally characterised by rapid decay of the magnetisation of the water protons which makes it difficult even to observe, let alone measure, its spatial distribution by MRI. In turn that restricts the scope of MRI to measure the mobility of the water molecules and thereby to characterise the pore structure of the matrix material. Nevertheless, the water in some porous matrices does have sufficiently long relaxation times for MRI to be able to make incisive practical studies. There is ample precedent for the use of Magnetic Resonance Imaging (MRI) to measure water content in a range of porous media including rocks [6,7,8,9], soils [10] and construction materials including bricks, cements and concrete [11,12].

All the tests described here were carried out on a modified Oxford Research Systems Biospec 1 spectrometer console and a 310 mm bore 2 Tesla superconducting solenoid magnet (Oxford Instruments). The coils used to produce the gradient fields have a 108 mm bore and give field gradients of 1.14 Gauss/mm. The radio frequency probe manufactured in HSLMC provides a

cylindrical space 54 mm in diameter and 163 mm long; the field-of-view is located in the central 100 mm. The images were acquired using a spin echo technique with an echo time T_E of 4.5 ms to enable efficient detection of the water proton signal. The relaxation time T_R ranged between 100 ms and 1000 ms depending on the type of observation; each measurement was taken 4 times and the results averaged. A spatial resolution of about 200 μm would allow the observation of fractures [13,14], although study of the pores within the matrix would require a higher resolution [13].

The MRI scanner provides spatial resolution by means of three sets of gradient coils, each of which produces a linear variation of magnetic field that induces a spatial distribution of the water proton resonance frequency in one of three orthogonal directions. The field of view was restricted to be 40 mm by 40 mm; a digital matrix of 256×256 pixels gives a resolution of 156 μm in both directions across a slice. The thickness of the slice can be chosen; 1250 μm was selected. In all the tests, what is being observed is the water, so the solid material shows up as a shadow.

3 IMAGING THE STRUCTURE OF CONCRETE

Due to the need for the sample to be in a very homogeneous magnetic field, MRI cannot be performed if there are any magnetic elements inside the sample; this precludes the use of steel reinforcement (but not FRP) and some types of aggregate. Figure 1 shows materials which are suitable for MRI, imaged in water. Both white limestone and quartz show the circularity of the beaker and the individual pieces of stone can be identified. Broken glass showed similar clarity. Unsuitable materials, such as granite, give distorted images.

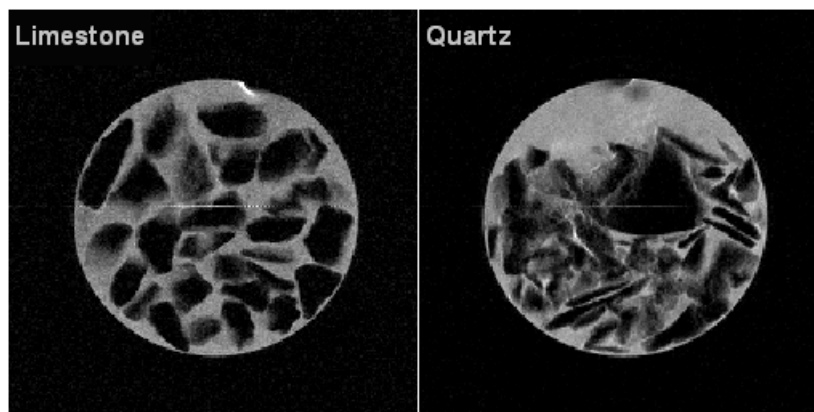


Fig. 1 Suitable materials for MRI (a) White limestone, (b) Quartz.

Ordinary Portland Cement contains a small amount of iron, which makes it unsuitable for MRI applications, but white PC contains no iron, and was found to give undistorted images. However, the water in concrete becomes bound as hydration proceeds. Figure 2 shows two images of the same sample; that after 8 hours shows less clarity and after 24 hours the aggregate cannot be distinguished.

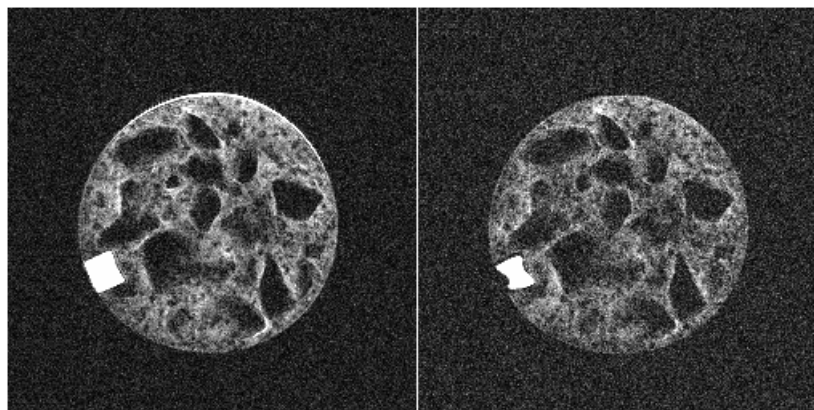


Fig. 2 The effect of hardening. (a) 1 hour after casting. (b) 8 hours after casting.

An attempt was made to make concrete with a matrix that contained 50% plaster of Paris, which is slightly porous and thus allowed the structure to be observed even after hydration had occurred. Figure 3 shows three images taken this way, two of which were taken after the concrete had been fractured. However, it was decided that this concrete did not behave in a way that was representative of normal concrete, and did not offer any advantage in terms of image analysis. Although both structure and fracture are visible in the same image, it is difficult to analyse, since both a small fracture and a piece of aggregate that partially fills the voxel would give the same level of grey and could not be distinguished.

As a result, it was decided to determine the structure of concrete by scanning the sample in the first few hours after casting, when there is sufficient free water to allow the individual pieces of aggregate to be observed.

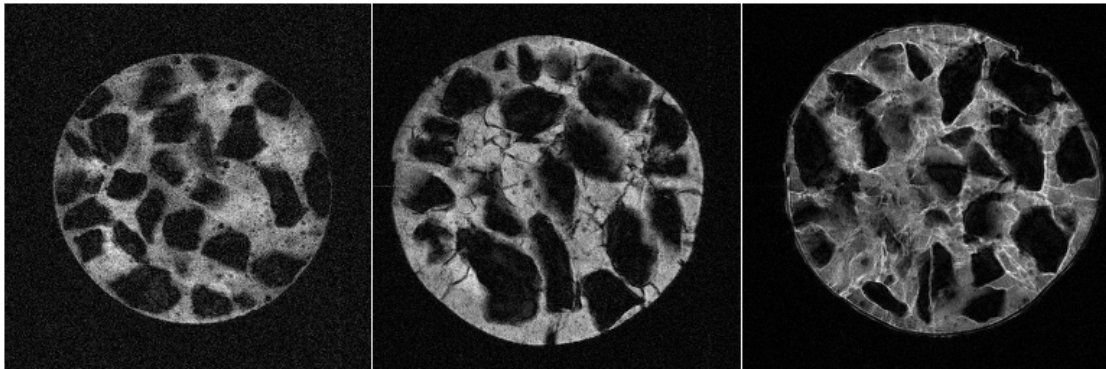


Fig. 3 Hardened saturated sample with 50 % plaster mix, (a) structure (b) air in fractures (c) water in fractures.

4 IMAGING FRACTURES IN CONCRETE

Fractures in small cylindrical concrete specimens, with and without external spiral reinforcement, were then observed. The specimens were first loaded and fractured outside the MRI scanner and following water saturation they were scanned in the unloaded state. Tests are also reported for a pull-out specimen in which the images of the resultant internal fractures are combined with images of the structure obtained before loading, to show that the relationship between the fractures and the individual pieces of aggregate can clearly be seen. Because of the need to avoid magnetic materials, Aramid Fibre Reinforced Plastic (AFRP) reinforcement was used.

The reinforcement used in the cylinder tests was made from Kevlar 49 aramid yarns [15]. Since these yarns do not yield and were not expected to break, their detailed properties are not of great importance; nevertheless their properties are given in Table 1. To produce a straight reinforcing bar, 10 yarns were coated with epoxy resin, twisted together and held straight in a jig until the epoxy had set. These rods were then tested in a tension testing machine to determine their strength and modulus. Predictably the strength is significantly less than the sum of the strengths of the yarns due to the difficulty in ensuring equal load sharing, but the modulus is closer to that of the yarns, since the loss of stiffness is caused only by misalignment, which is slight [16]. Such bundle effects are well known [17] and would be reduced if the rods were made by machine that would enable better quality control. The spirals used to provide the lateral confinement of the cylindrical specimens were made in a similar way; six yarns were wrapped around cylindrical formers immediately after twisting them together. Tensile tests were not carried out on these specimens, but it is to be expected that their strength and stiffness would be similar to those of the straight specimens.

Table 1 Yarn and AFRP properties (based on fibre area).

	Strength (MPa)	Fibre area (mm ²)	Modulus (GPa)	Strength (N)
Kevlar 49 yarn	2640	0.168×10^{-6}	120	445
10 yarn AFRP rod	2100	1.68×10^{-6}	120	3520

The concrete specimens were cast into plastic beakers which were left in place during the testing since they prevented the specimens drying out, and ensured that the fragments did not fall apart after the specimens had been loaded. The beakers were thin and flexible and are not believed to have had significant effect on the behaviour of the samples under load.

4.1 Axially-loaded specimens

Figure 4 shows 2D MRI slice scans taken axially and transversely through confined and unconfined specimens. The image intensity has been inverted (so the presence of water is shown as black, instead of white as in the original images), and the range of grey levels has been adjusted in order to aid reproduction in publication. The unconfined sample has a major fracture propagating at an angle of about 21° to the loading axis; in contrast, the confined sample shows fractures at about 21° to the transverse direction which indicates that the passive loading from the confining spirals is also very significant. The transverse scan shows circular and radial fracture surfaces for the unconfined sample, which means that the fracture has propagated as a cone from one end, whereas the confined sample shows a square pattern, which is directly related to the location of the reinforcement.

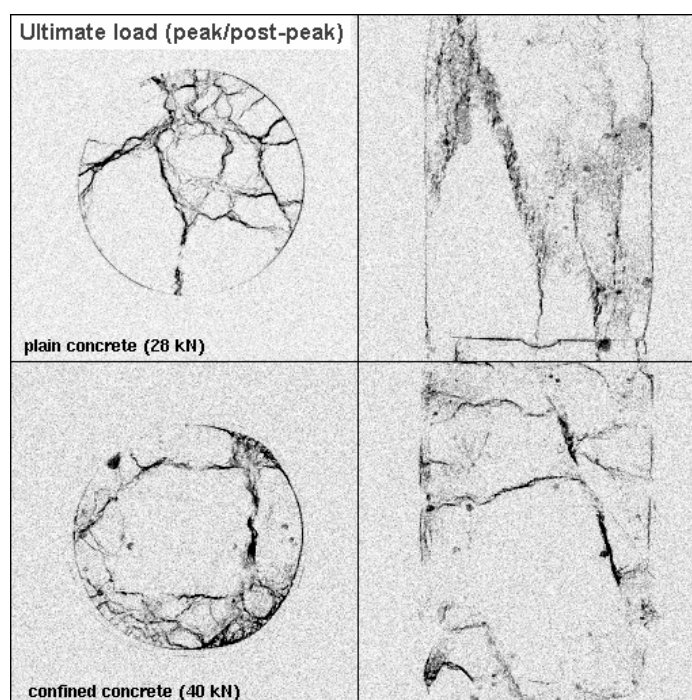


Fig. 4 Images of slices through concrete samples after the ultimate load has been reached; (top) unconfined, (bottom) confined.

It should be noted that these images are the last in sequences that have been obtained, on the same samples, after the application of different load levels. Because the technique is non-destructive, the growth of fractures can be studied over time. It should also be noted that these images are part of a 3D data set that can be viewed with suitable software and rotated or zoomed as required.

4.2 Pull-Out Specimens

It is desirable to be able to compare structure and fracture images of the same specimen. The pull-out samples were scanned under conditions to enable image-coregistration. Figure 5 shows the result; these images have not been inverted, nor have the grey scale levels been adjusted. The top row shows slices through the sample at a level where the rod was bonded to the concrete; the bottom row shows slices where the rod and the concrete were debonded by means of a plastic sleeve. In each row, the image on the left shows the sample as scanned while curing; the AFRP rod shows as a circular black dot since it contains virtually no water, and the registration square (which was made from raw potato, which is full of water but which maintains its shape) is also clearly visible on the left hand side. In the lower image the edges of the plastic sleeve can be seen. The central scans show the sample after it was loaded in a tension testing machine to pull out the AFRP rod. The hole left by

the AFRP rod has filled with water, as have both the cracks which join the rod to the surface and the other cracks that occur internally. The registration square is also clearly visible; the potato itself has shrunk by osmosis but the space it left has been filled with water. The images on the right show the two images rotated, registered and superimposed. The relative position of the aggregate and the fractures is clear; some of the fractures skirt round the aggregate pieces, but some of the cracks pass through larger pieces of aggregate. This black and white reproduction is less clear than is possible if colour can be used, since contrasting colours can be assigned to the water in the two images.

It is possible to automate the process of detecting the cracks. The image can be segmented by selecting only a narrow range of grey levels to eliminate extraneous detail and then using edge-detection algorithms to delineate the major fractures. Some resolution is lost in this process, and the optimisation parameters are currently being studied, but the potential benefits of applying these techniques to large 2D and 3D data sets is clear.

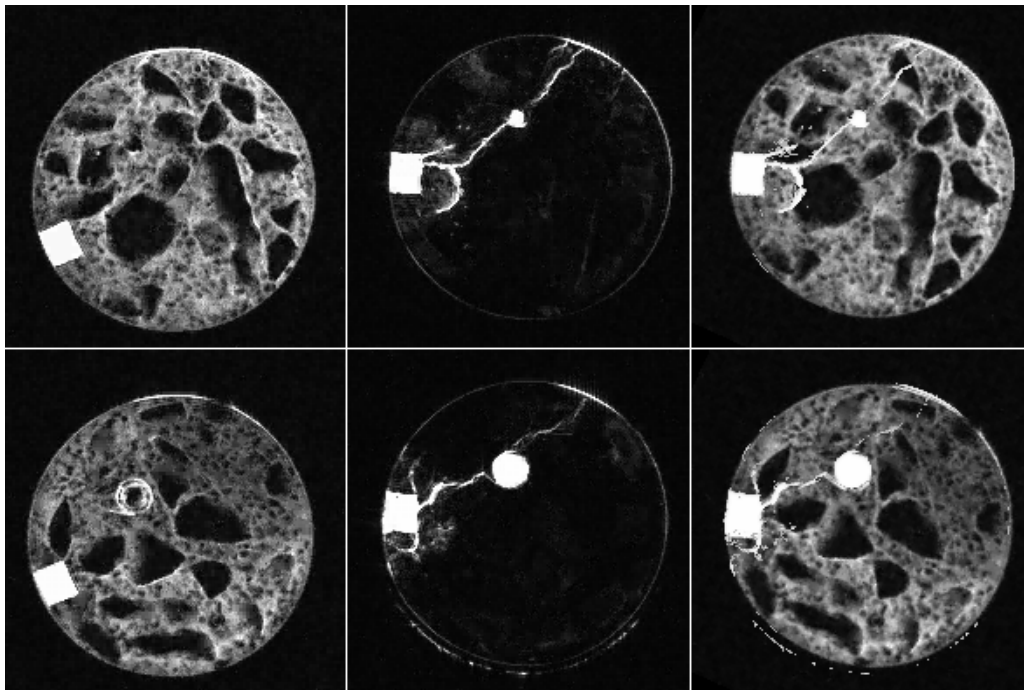


Fig. 5 Pull-out specimen. Top row – slices through sample where rod is bonded to concrete. Bottom row – slices through sample where rod is sleeved. In each row, image on left obtained before testing; central image showing fractures; images on right show the two images superimposed.

4.3 In-situ beam test

To demonstrate the power of the techniques, an experiment was carried out which allowed a beam to be loaded *inside* the MRI machine so that scans could be made while the beam was under load. Space was extremely limited; the beam, and its test frame, neither of which could contain any iron, had to be built around the radio-frequency antenna and fitted within a cylinder 108 mm in diameter. The beam, which was 570 mm long, 30 mm deep and 25 mm wide, is shown in Figure 6. The test frame was made from nylon bars and polycarbonate sheet, with twisted aramid yarns as the tension elements. The load was applied using medical syringes driven backwards as hydraulic jacks, and the beam was contained in a water tank which was filled while the beam was being loaded, so that the fractures filled with water, and then drained before scanning so that the signal from the water in the tank did not overwhelm that from within the fractures. Figure 7 shows the complete rig ready for placing in the scanner. Full details of the test arrangement are described elsewhere [3].

The reinforcement for the beam was made from AFRP; the reinforcement cage is shown in Figure 8. Eight yarns were drawn through a bath of epoxy resin and lightly twisted together to form a bar; excess resin was removed and the bar kept under light tension while the epoxy hardened. Tests showed that 8-yarn bars had a tensile strength of 2380 MPa and a modulus of 120 GPa. The strength conversion efficiency from yarns to bars of 82% is typical of what can be achieved by hand; with machine-made pultrusions, higher efficiencies can be achieved.

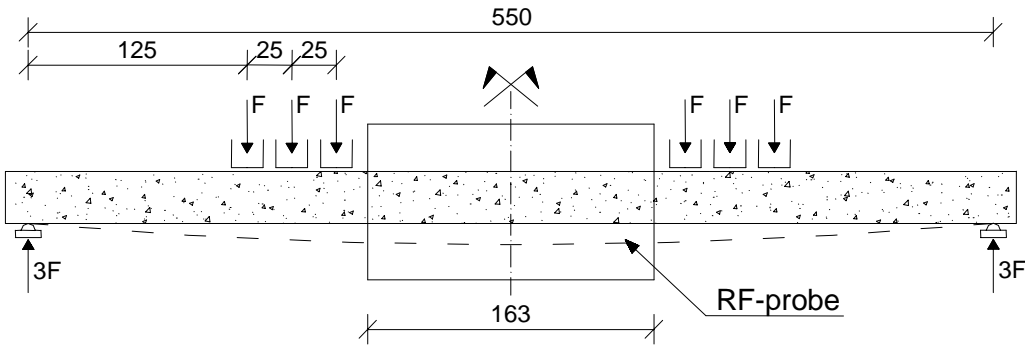


Fig. 6 Beam loading arrangement (dimensions in mm).



Fig. 7 Assembled frame ready for installation in the MR magnet.

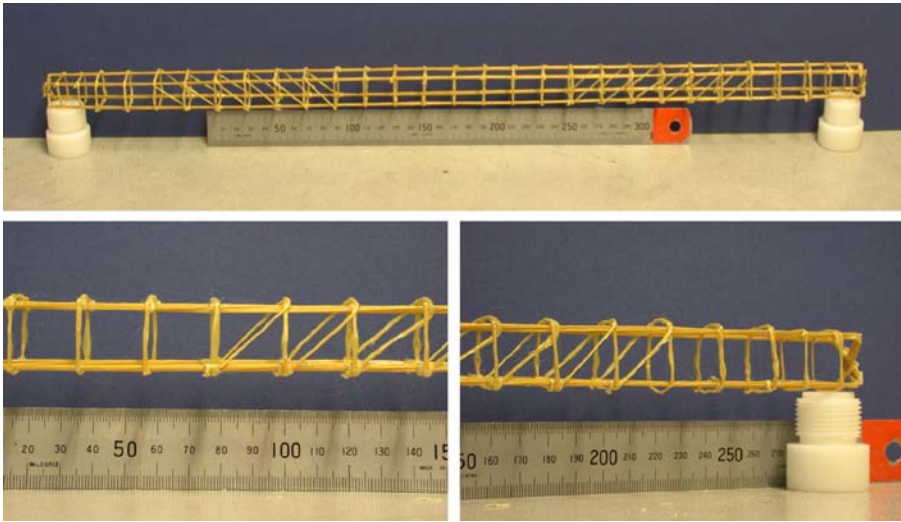


Fig. 8 Details of AFRP beam reinforcement.

The concrete mix used sieved white limestone aggregate of various sizes, white cement and deionised water; this mix had been found to be satisfactory in earlier tests using MRI. The effective cube strength of this mix, on the scale used in these experiments [18], was about 30 MPa. AFRP reinforcement has a virtually linear stress-strain curve to failure; the ultimate moment capacity is governed by the strength of the FRP and was calculated to be 93 Nm.

The earlier studies had shown that the internal structure of concrete can be measured by MRI during the first eight hours after casting. A set of scans was taken immediately after casting; these scans did not need either the loading system or tank in place, so it was relatively easy to reposition the beam inside the scanner; the whole beam was scanned in 70 mm lengths with about 20 mm overlap.

The beam was cured under water for four weeks in the laboratory; the beam and test rig were then assembled and placed into the scanner as described above. Before loading, a scan of the central region was carried out to detect any pre-existing fractures or voids. The beam was then loaded monotonically, and the following procedure was adopted for each set of readings:

- The beam was submerged by filling the external tank with water.
- The chosen load was applied by adding concrete weights to the loading system
- The adjustable loading stop was used to fix the displacement of the load; this prevented any further displacement of the beam.
- The external tank was drained to remove the surrounding water.
- The MRI scan was carried out, taking about 7 hours; the data were then archived and processed after scanning.

Because the complete experiment would take several days, and it would be impossible to adjust the specimen once it was inside the MRI scanner, the entire process was tried out on a second beam outside the scanner so that potential problems could be identified before the real test was carried out; no significant alterations were required.

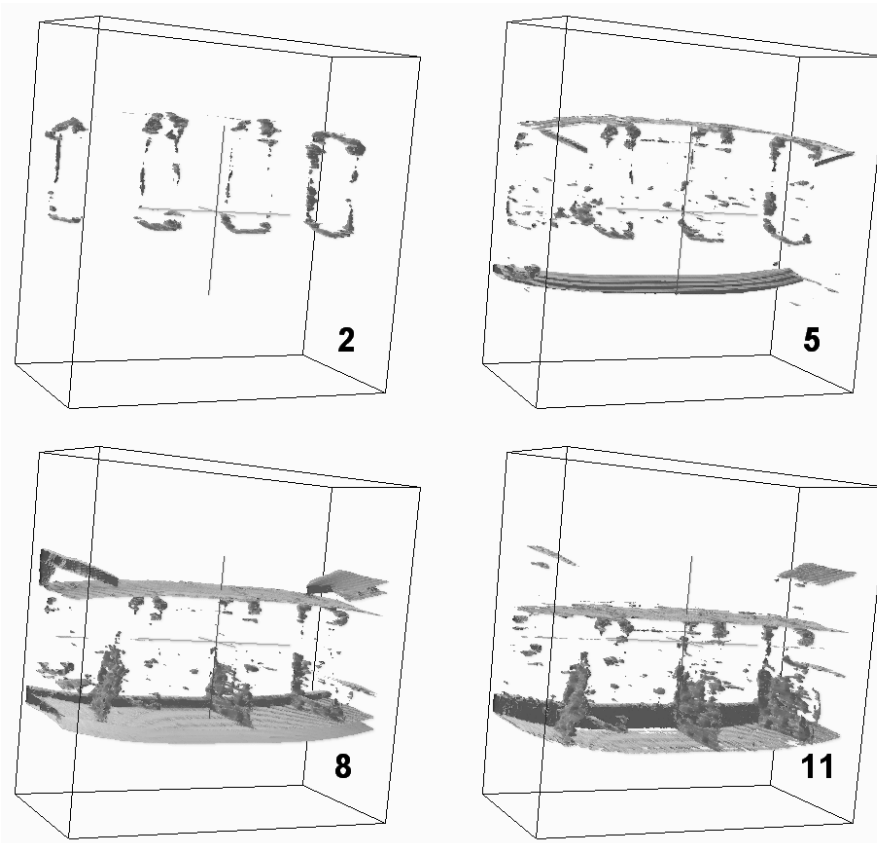


Fig. 9 3D observation of the fracture at four different loading stages. In image 2, the water that has been detected is in the adhesive in the shear links; the later images show more water filling the expanding cracks.

Figure 9 shows a 3D reconstruction of images that have been processed to remove all voxels that are darker than a certain threshold; this is effectively a 3D map of the spaces inside the concrete that contain water. Pre-existing voids around the shear reinforcement are clearly visible, which may be caused by incomplete compaction around the stirrups. Since the slice thickness was about 10 times the in-plane pixel size, the vertical shear links and the longitudinal reinforcement are less clearly delineated. These images clearly show the growth of the cracks from the bottom surface of the beam and they also show that some cracks form at the shear links' positions, whereas others form between the shear links.

In this particular loading case there is no overall shear force in the beam within the field of view, and as expected, the cracks appear primarily as vertical surfaces extending to the neutral axis of the beam. However, local stress concentrations around aggregate and reinforcement can cause local stress variations, and this causes the cracks to diverge from the overall vertical alignment. This can be clearly seen in the expanded 2D slices shown in Figure 10 of the region where one of the cracks forms away from the shear link; the crack appears to be diverted horizontally around a relatively large piece of aggregate and details of the fracture propagation can be clearly observed. These images have been co-registered spatially to eliminate the gross movement caused by beam deflection, using the sections through the shear reinforcement as reference marks; the fracture image has been enhanced to eliminate the grey background.

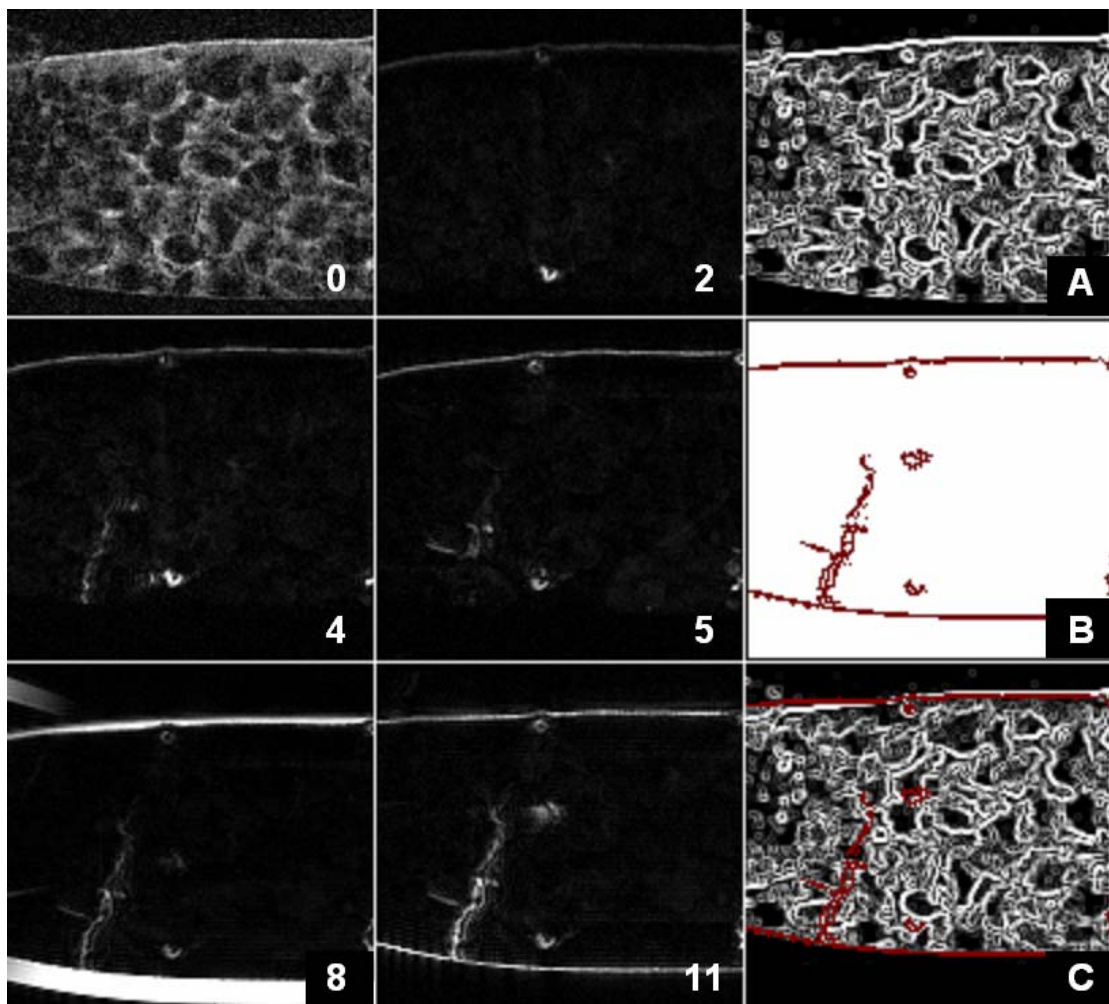


Fig. 10 Enlarged details of one crack at different loading stages. Images 0, 2, 4, 5, 8, 11 show successive loading stages of the area. Image A shows edge detection applied to image 0; Image B shows edge-detection applied to image 11; Image C shows the two images superimposed.

5 CONCLUSIONS

It has been shown that the use of AFRP reinforcement, combined with innovative MRI techniques, can be used to investigate the behaviour of reinforced concrete on the meso-scale. MRI imaging detects the presence of water and is most sensitive to free water that is not bound, either physically or chemically. It has been necessary to use materials in the concrete that do not interfere with the magnetic fields used in the scanner; granite, and at least some river gravels, are unsuitable, but white limestone and quartz are suitable, as are silica sands.

Liquid-state MRI, using a spin echo protocol with an echo time of 4.5 ms, and a repetition time of 100 ms has been found to be suitable; for a 2D slice 1.25 mm thick a spatial resolution of $156 \times 156 \mu\text{m}$ has been attained, using a 256×256 digital matrix; four measurements have to be taken of each signal and averaged and the total scan time is 1.7 minutes. Alternatively, a 3D image set $156 \times 156 \times 1250 \mu\text{m}$ requires 55 minutes of scanning time.

Although OPC contains only a small amount of iron, it is unsuitable as a cementing material for MRI studies, whereas WPC has been shown to give clear images. It is possible to see the structure of concrete for a few hours after casting, but as the water becomes bound to the cement surface, or reacted to form hydroxides, it becomes almost invisible. Plaster of Paris has also been shown to give clear images, and as it is slightly porous, it allows the structure to be observed even after hardening. This visibility persists when a small proportion of plaster is mixed with WPC, but the plaster significantly alters the fracture process in the resultant concrete which is not representative of structural concrete.

It has been concluded that it is not feasible to obtain a single image that distinguishes aggregate, matrix and fractures. This is partly because the MRI visibility of the structure decreases as hardening takes place, and partly because, when both matrix and fractures are present in the same image it is difficult to distinguish between them because they both show up as different levels of grey. Thus, it is preferable to take one image which clearly shows the structure, and subsequently a second image to show the fractures in high contrast from the solid components. This is a key strategic innovation of this study since it enables MRI to be used to study both the internal geometry of a concrete sample to locate internal defects and also to measure fractures subsequently induced. MRI can also be used to study the hardening of concrete samples, and, by observing the water content, allows studies of the chemistry of cement and concrete.

Cylindrical concrete specimens, either unreinforced or constrained by spirals of AFRP, have been cast and tested in axial compression and it has been demonstrated that MRI provides a non-destructive method for measuring fractures within a hardened concrete sample. It is feasible for the same sample to be scanned before, during, and after a loading sequence, so the progress of fracture generation can be measured. Although this was always intended to be a proof-of-concept study, it nevertheless clearly demonstrates the difference in internal crack structure between plain and reinforced specimens.

Since it is possible to relate images of the fractured samples to those of the concrete structure obtained soon after casting, the relationship between fractures and the aggregate structure within the concrete can be observed. Such comparisons are facilitated if markers are inserted into the concrete samples such that the different images can be accurately related to one another. It is also possible to combine MR images using 3D image reconstruction software, which makes it feasible to study solid models of both the structure and fractures within the concrete.

The study has demonstrated how a test frame can be assembled inside a MRI scanner to enable scans to be made while the specimen is under load. Since the testing method is non-destructive, it is possible to follow the progress of fracture as the loading increases.

In the light of all these factors it is now clear that MRI is a powerful, non-invasive tool for studies of the meso-structure of concrete. MRI provides a non-invasive experimental approach to observe the progress of fracture during laboratory testing, and as a result it is now possible to design experiments to measure fracture processes in flexure, shear, bond, confinement or impact. This can be achieved either by using devices designed to load the specimen inside the MRI machine, or to use test procedures that allow samples to be loaded outside the MRI machine, and then enable the series of independently scanned images to be spatially correlated with one another.

To the best knowledge of the authors, MRI scanning is the only non-destructive technique for direct observation and quantitative measurement of internal crack structures in such detail, and it is believed that this study is the first to demonstrate the procedures.

ACKNOWLEDGEMENTS

This work was supported by the EU TMR Network "ConFibreCrete" and by the Herchel Smith Endowments.

REFERENCES

- [1] Marfisi E., Burgoyne C.J., Amin M.H.G. and Hall L.D., The use of MRI to observe the structure of concrete, *Magazine of Concrete Research*, 52, 101-109, 2005.
- [2] Marfisi E., Burgoyne C.J., Amin M.H.G. and Hall L.D., The use of MRI to observe the fracture of concrete, *Magazine of Concrete Research*, 52, 111-121, 2005.
- [3] Marfisi E., Burgoyne C.J., Amin M.H.G. and Hall L.D., Observation of flexural cracks in loaded concrete beams using MRI, *Magazine of Concrete Research*, 52, 225-234, 2005.
- [4] Mansfield P and Morris PG, *NMR Imaging in Biomedicine*, Academic Press, London, 1982.
- [5] Callaghan P.T., *Principle of Nuclear Magnetic Resonance Microscopy*, Clarendon Press, Oxford, 1991.
- [6] Gummerson R.J., Hall C., Hoff W.D., Hawkes R., Holland G.N. and Moore W.S., Unsaturated water flow within porous materials observed by NMR imaging, *Nature*, 281, 56-57, 1979.
- [7] Carpenter T.A., Davies E.S., Hall C., Hall L.D., Hoff W.D., Wilson M.A., Capillary water migration in rock: Process and material properties examined by NMR Imaging, *Materials and Structures*, research and testing, 26, 268-292, 1993.
- [8] Kleinberg R.L., Straley C., Kenyon W.E., Akkurt R. and Farooqui S.A., Nuclear magnetic resonance of rocks: T_1 vs T_2 , *SPE paper 26470*, SPE International, 1993.
- [9] Kleinberg, R. L., W. E. Kenyon, and P. P. Mitra, Mechanism of NMR relaxation of fluids in rock, *J. Magn. Reson., Series A*, 108, 206-214, 1994.
- [10] Hall, L. D., Amin M. H. G., Dougherty E., Šanda M., Votrubová J., Richards K.S., Chorley R.J., Císlarová M., MR properties of water in saturated soils and resulting loss of MRI signal in water content detection at 2 tesla, *Geoderma*, 80, 431-448, 1997.
- [11] Kaufmann J., Stunder W., Link J., Schenker K., Study of water suction of concrete with Magnetic Resonance Imaging methods, *Magazine of Concrete Research*, 49, 157-165, 1997.
- [12] Valckenborg R.M.E., Pel L., Hazrati K., Kopinga K., Marchand J., Pore water distribution in mortar during drying as determined by NMR, *Materials and Structures*, 34, 599-604, 2001.
- [13] van Mier J.G.M., *Fracture processes of concrete - assessment of material parameters for fracture models*, CRC Press, 1997.
- [14] Wittmann F.H. , *Fracture mechanics of concrete*, Elsevier, *Developments in Civil Engineering* 7, 1983.
- [15] Burgoyne C.J., Aramid fibres for civil engineering applications, in *Construction Materials Reference Book*, ed. D.K.Doran, Butterworths, 1992.
- [16] Amaniampong G. and Burgoyne C.J., Statistical variability in the strength and failure strain of aramid and polyester yarns. *Journ. Materials Science*, 29, 5141-5152, 1994.
- [17] Daniels H.E., The Statistical strength of bundles of threads I, *Procs Roy. Soc. London*, A183, 45-70, 1945.
- [18] Ahmed E. Ahmed, Does core size affect strength testing?, *Concrete International*, 21/8, 35-39, 1999.